# Electronic Supplementary Information

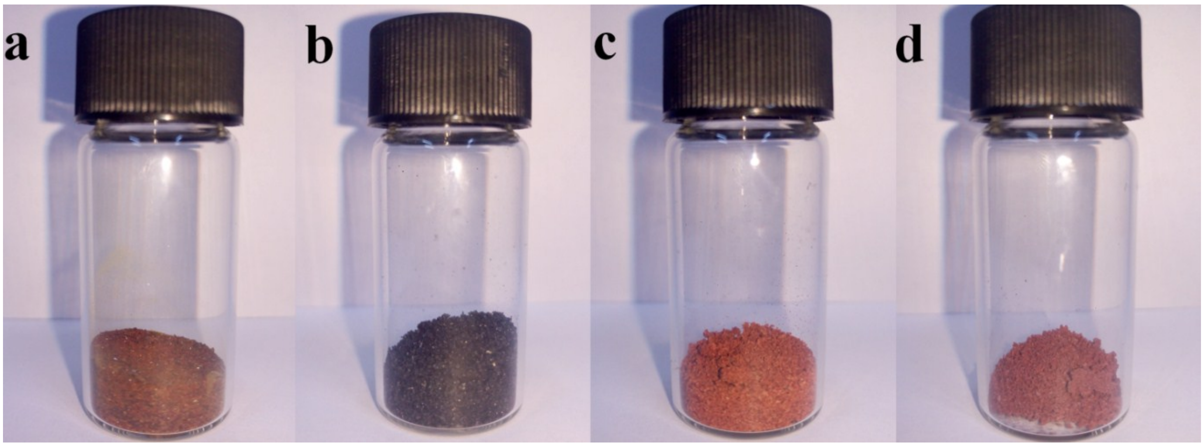


**Fig. S1.** Photographs of (a) the mixed PVP + $Fe(NO_3)_3{\cdot}9H_2O$ powder after drying at 80 $^oC$ overnight. (b) As-collected $Fe_xO$@NFLG-240 product. (c) As-collected $Fe_2O_3$@NFLG-300 product and (d) as-collected $Fe_2O_3$@NFLG-900 product.

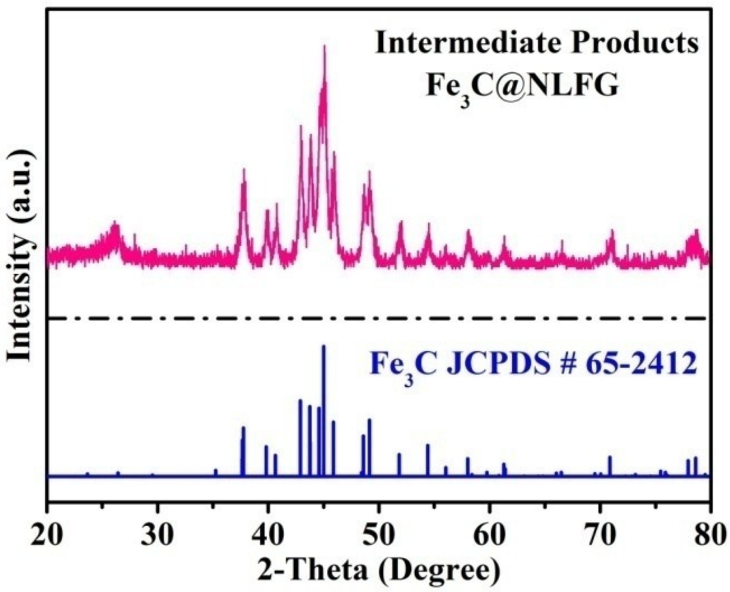


**Fig. S2.** XRD pattern of $Fe_3C$@NFLG as intermediate products before in-situ oxidation treatment during the synthesis of $Fe_xO$@NFLG-240.

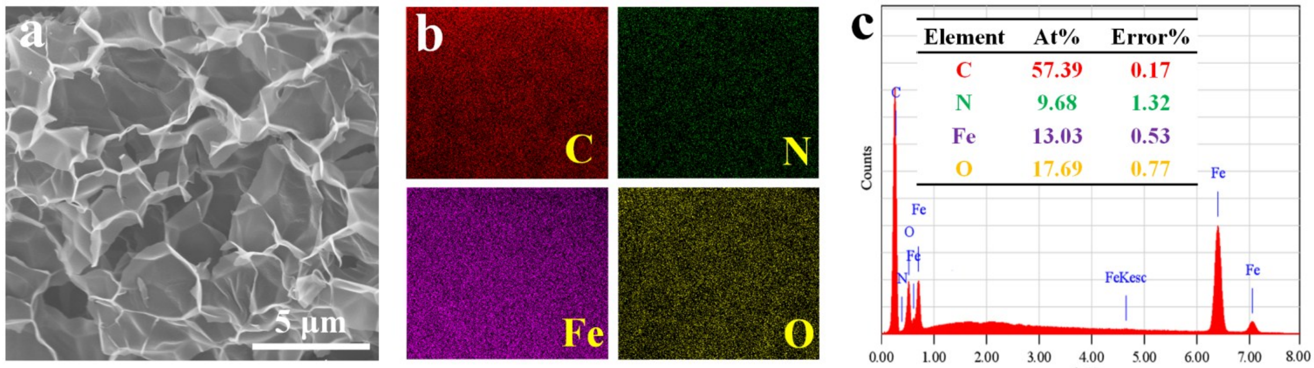


**Fig. S3.** (a) SEM image, (b) corresponding EDS elemental mappings C, O, Fe and N element, (c) corresponding EDS spectrum of $Fe_xO$@NFLG-240.

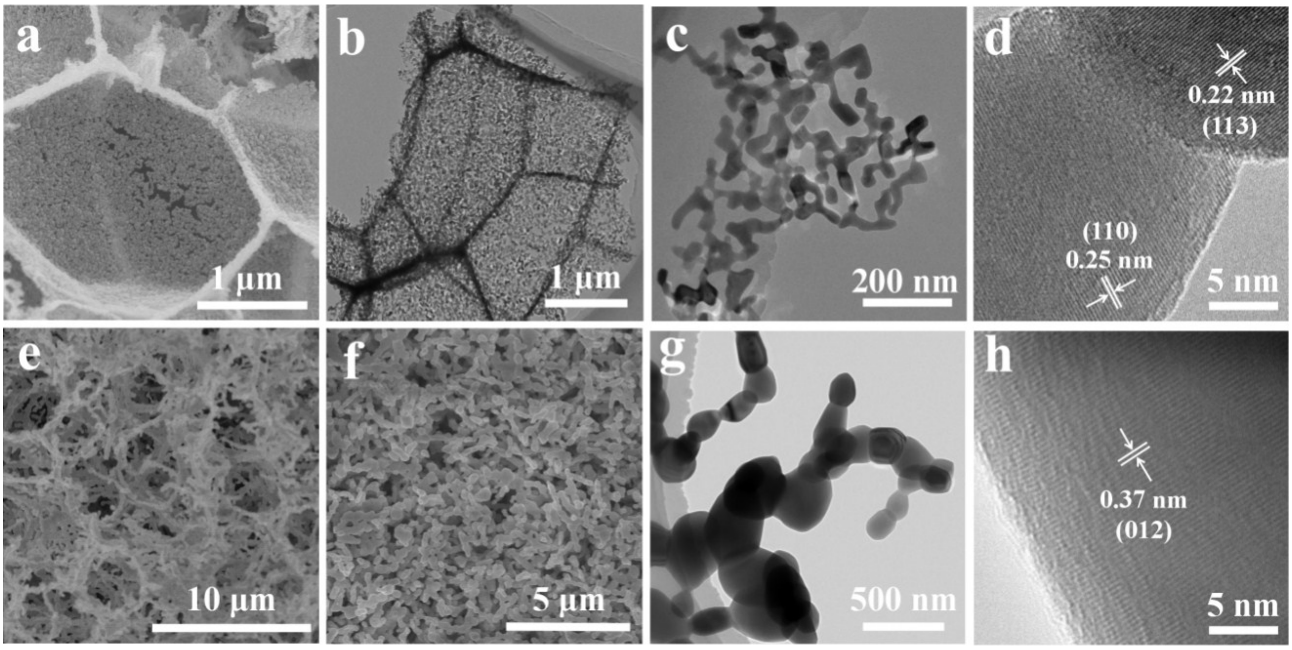


**Fig. S4.** Morphological analysis of (a) SEM images, (b) TEM images of low magnification and (c) high magnification, (d) high resolution lattice fringe image of $Fe_2O_3$@NFLG-300. (e) and (f) SEM images and (g) TEM images of low magnification and (h) high resolution and lattice fringe image of $Fe_2O_3$@NFLG-900.

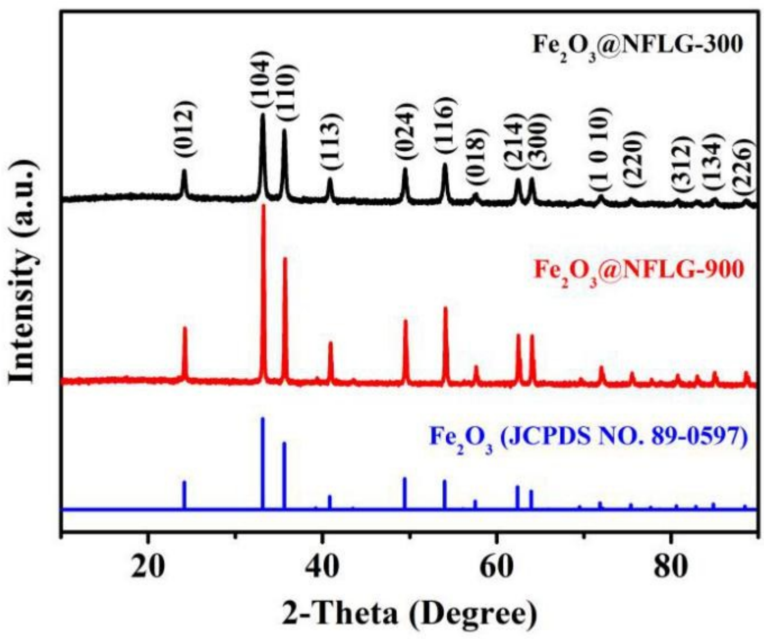


**Fig. S5.** XRD patterns of $Fe_2O_3$@NFLG-300 and $Fe_2O_3$@NFLG-900.

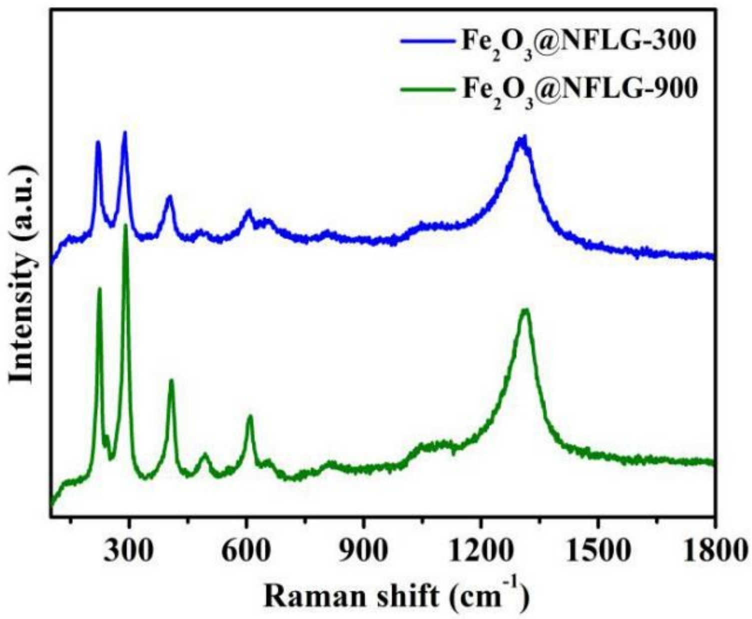


**Fig. S6.** Raman spectra of $Fe_2O_3$@NFLG-300 and $Fe_2O_3$@NFLG-900.

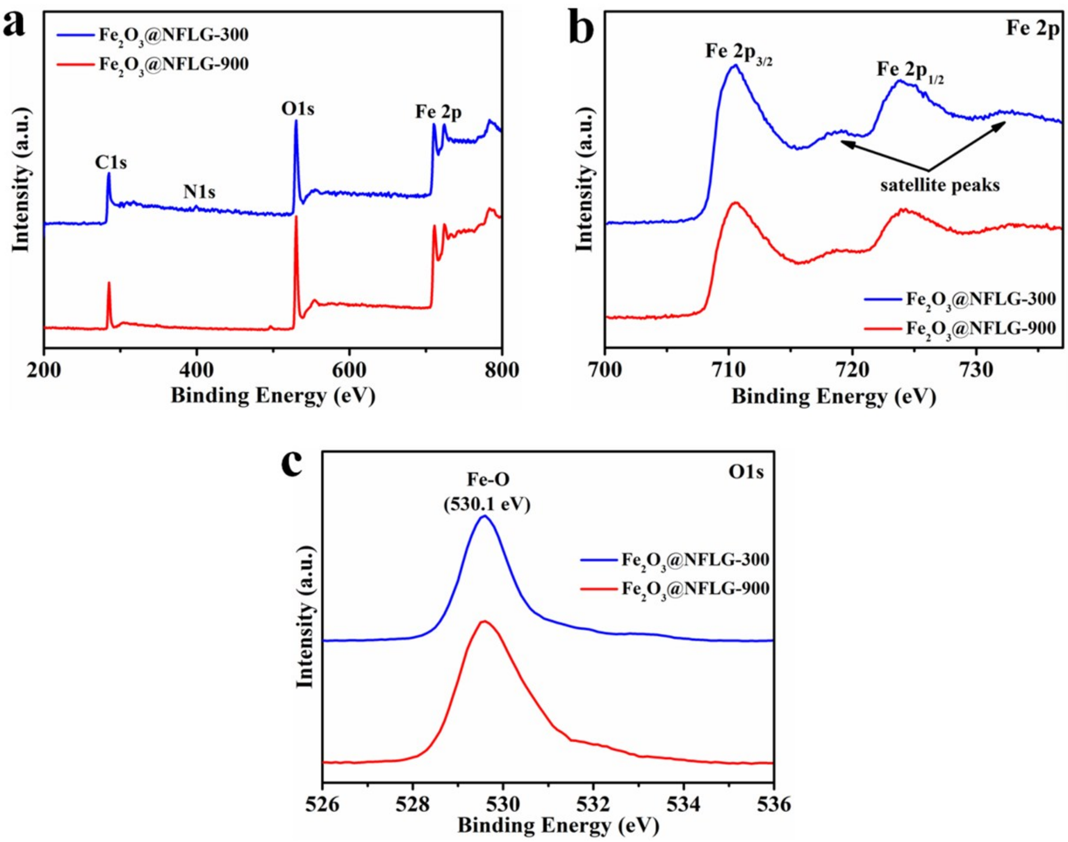


**Fig. S7.** XPS spectra of (a) full survey profiles, (b) High resolution Fe 2p spectra and (c) High resolution O 1s spectra for $Fe_2O_3$@NFLG-300 and $Fe_2O_3$@NFLG-900.

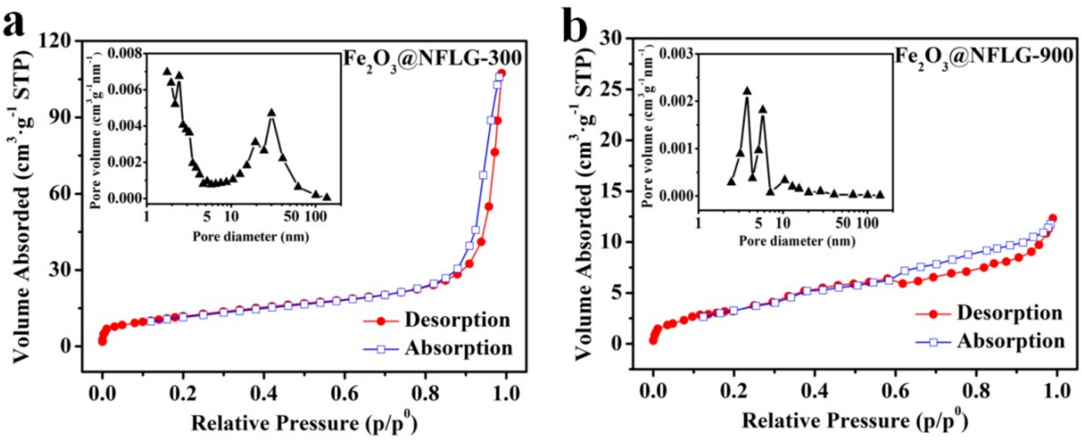


**Fig. S8.** Nitrogen adsorption–desorption isotherms and pore size distributions (inset) of (a) $Fe_2O_3$@NFLG-300 and (b) $Fe_2O_3$@NFLG-900.

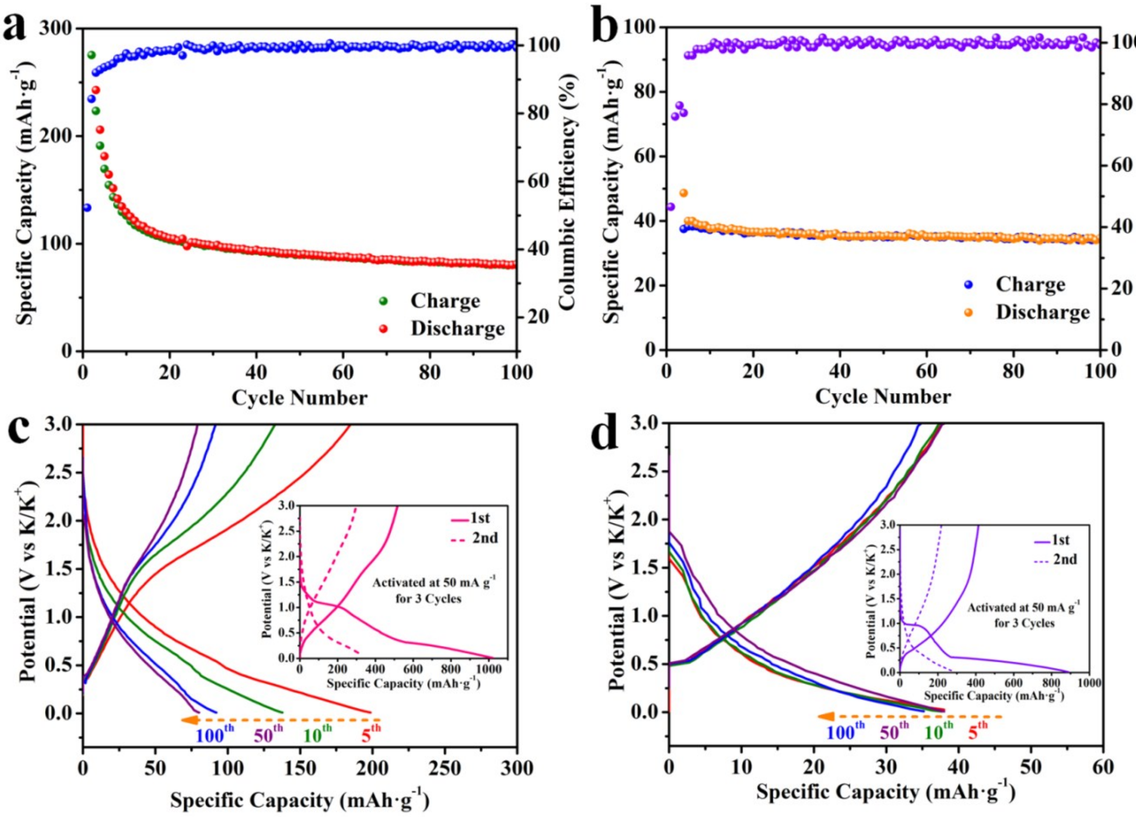


**Fig. S9. Electrochemical performance of potassium-ion batteries.** (a) Reversible specific capacity and coulombic efficiency and (b) potential versus specific capacity for $Fe_2O_3$@NFLG-300 electrode during different cycles at 1.0 A $g^{-1}$, (c) Reversible specific capacity and coulombic efficiency and (d) potential versus specific capacity for $Fe_2O_3$@NFLG-900 during different cycles at 1.0 A $g^{-1}$.

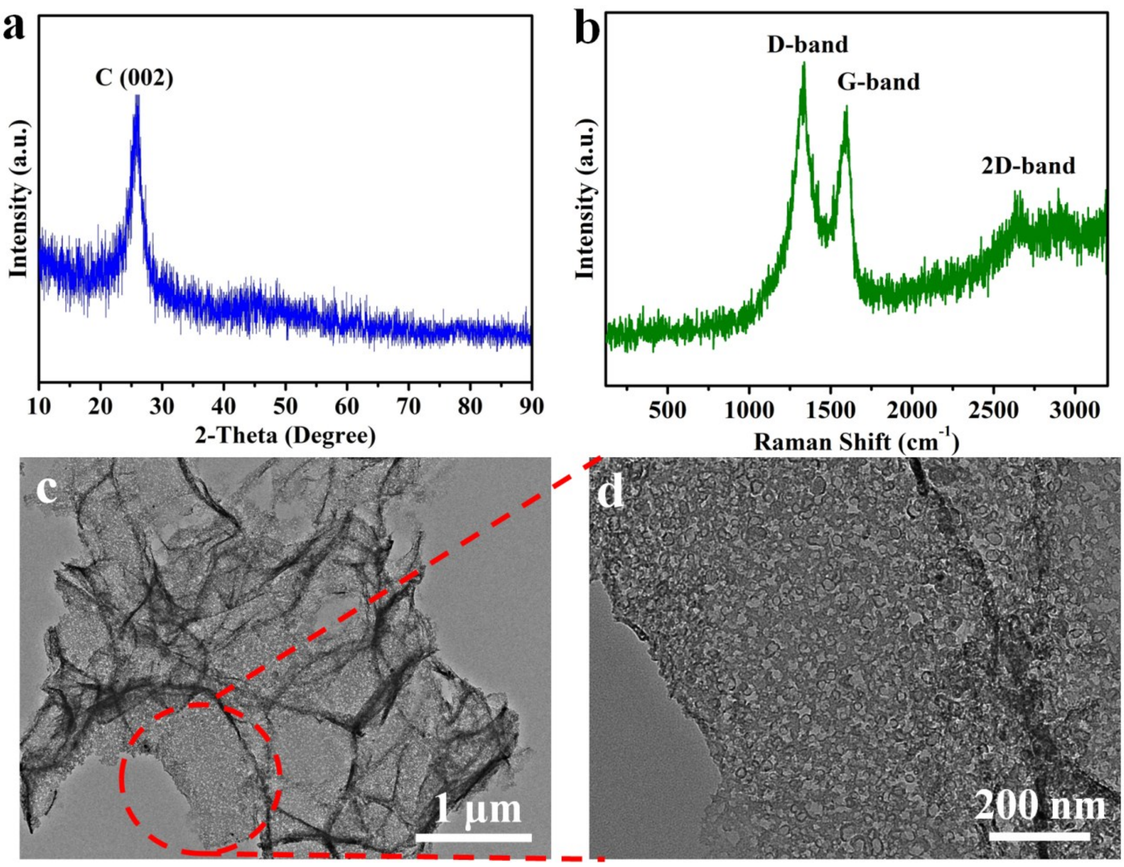


**Fig. S10.** (a) XRD profile, (b) Raman spectrum, (c) Low magnification and (d) High magnification TEM images of 3D-NFLG.

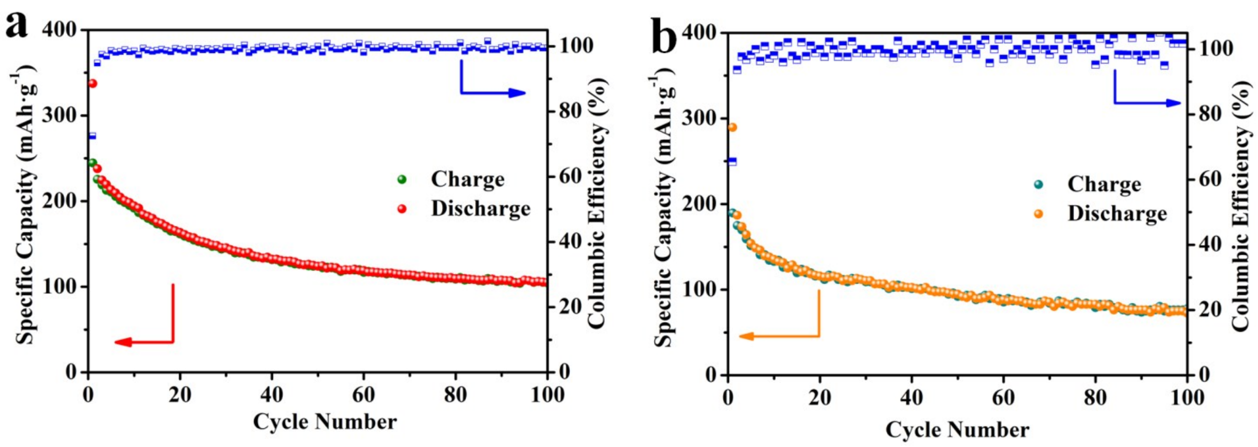


**Fig. S11.** Cycling performance of 3D-NFLG at a current density of (a) 2 A g$^{-1}$ and (b) 5 A g$^{-1}$ for 100 cycles.

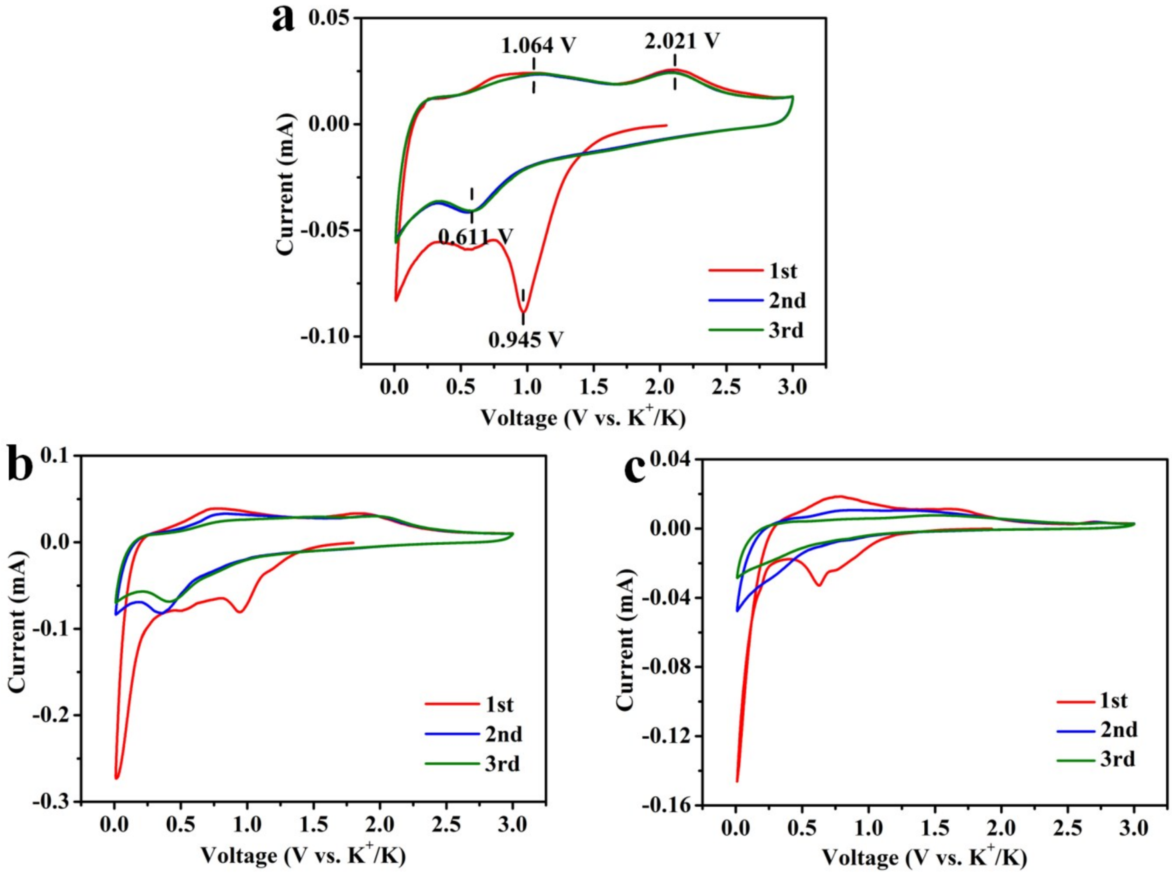


**Fig. S12.** Cyclic Voltammetry profiles of (a) $Fe_xO$@NFLG-240, (b) $Fe_2O_3$@NFLG-300 and (c) $Fe_2O_3$@NFLG-900 recoded at a sweep rate of 0.1 mV $s^{-1}$ between 0.01 and 3.0 V (versus $K^+$/ K).

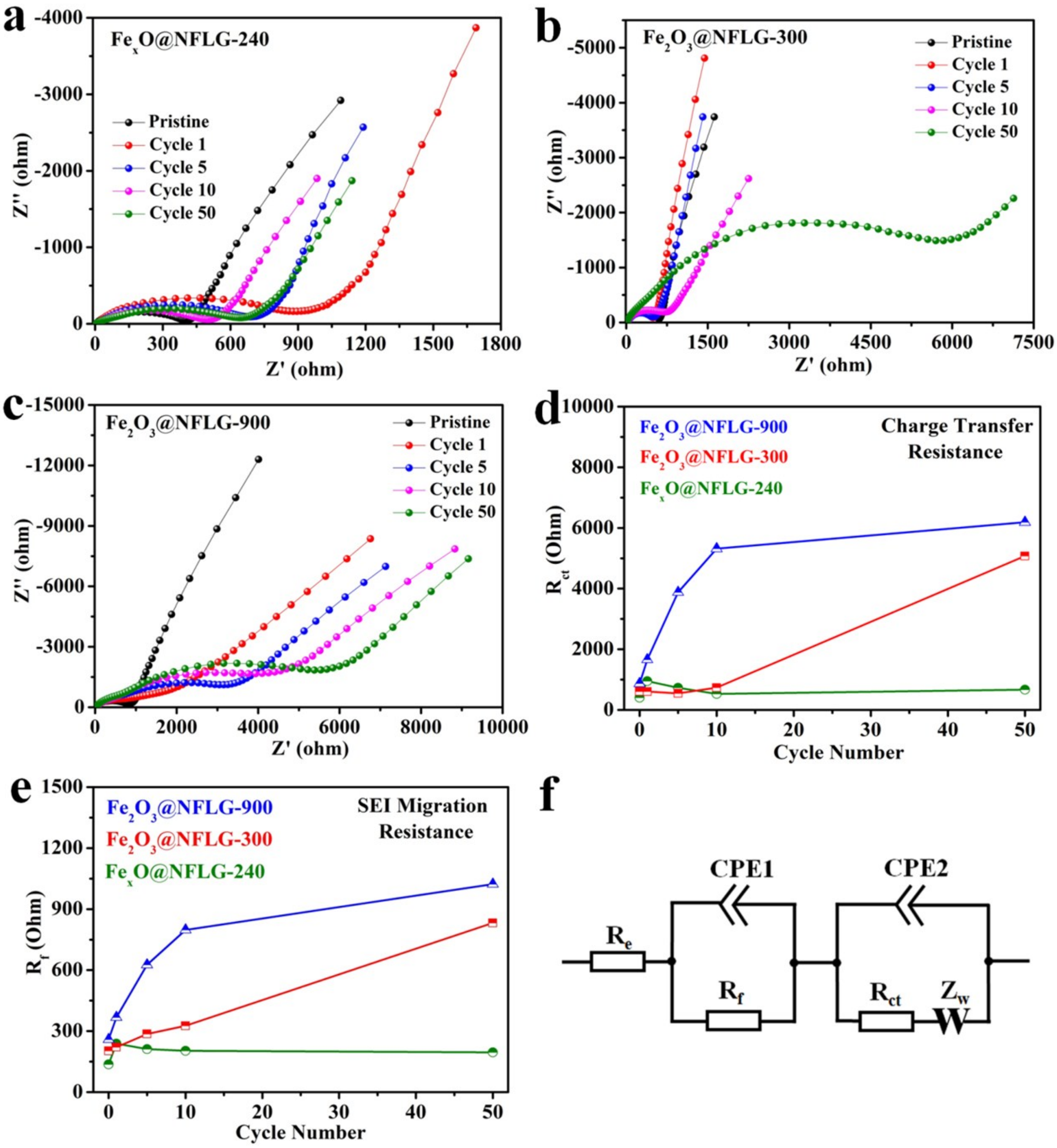


**Fig. S13.** Nyquist plots of (a) $Fe_xO$@NFLG-240, (b) $Fe_2O_3$@NFLG-300 and (c) $Fe_2O_3$@NFLG-900 electrodes after various cycles. The fitted impedence parameter of (d) $R_{ct}$ and (e) $R_f$ for $Fe_xO$@NFLG-240, $Fe_2O_3$@NFLG-300 and $Fe_2O_3$@NFLG-900 electrodes versus cycle numbers. (f) The equivalent circuit model used for fitting the Nyquist plots.

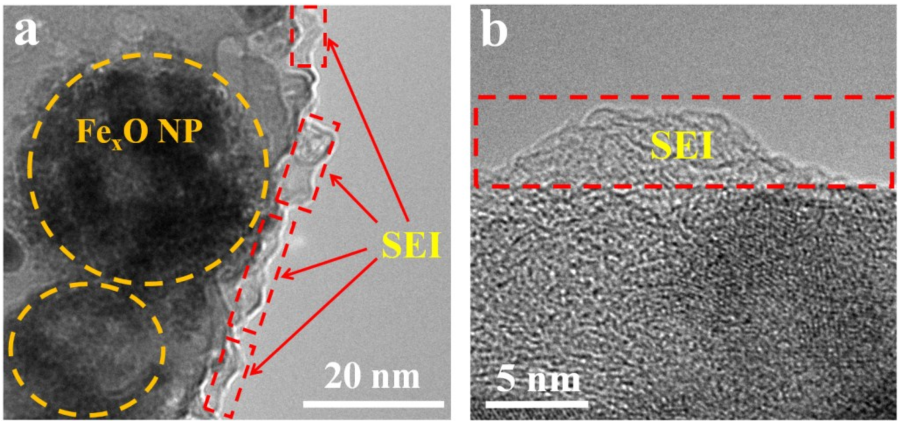


**Fig. S14.** (a) Ex situ TEM image of $Fe_xO$@NFLG-240 electrodes after 100 cycles at 2 A $g^{-1}$. (b) HRTEM image of the cross sectional profile of SEI layer covered on the edge of the graphene nanosheet.

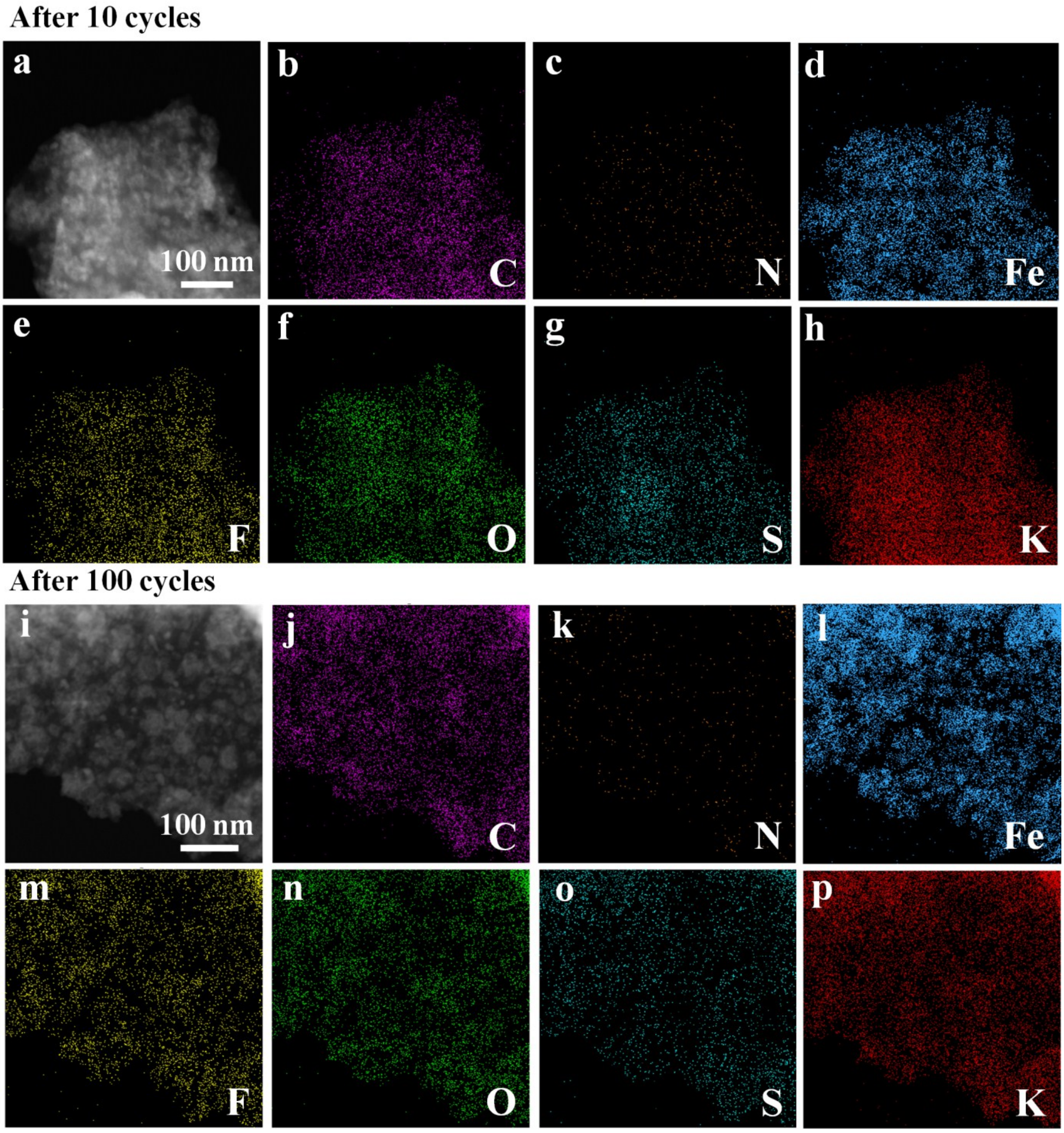


**Fig. S15.** Ex situ STEM image of $Fe_xO$@NFLG-240 electrodes after (a) 10 cycles at 2 A $g^{-1}$ and corresponding EDS elemental mappings of (b) C, (c) N, (d) Fe, (e) F, (f) O, (g) S and (h) K. (i) after 100 cycles at 2 A $g^{-1}$ and corresponding elemental mappings of (j) C, (k) N, (l) Fe, (m) F, (n) O, (o) S and (p) K.

**Table S1.** Elemental composition analysis results of $Fe_xO$@NFLG-240, $Fe_2O_3$@NFLG-300 and $Fe_2O_3$@NFLG-900 by ICP and C-S analysis.

| Element | Weight Percentage (wt.%) | | |
|---|---|---|---|
| | $Fe_xO$@NFLG-240 | $Fe_2O_3$@NFLG-300 | $Fe_2O_3$@NFLG-900 |
| Fe | 47.0 | 68.3 | 70.6 |
| C | 29.6 | 1.26 | 0.032 |
| N | 1.15 | 0.39 | 0.18 |
| O | ≥20 | ≥20 | ≥20 |

**Table S2.** Electrochemical performance of recently reported anode materials for potassium ion batteries.

| Material | Rate Capability | Cyclability (capacity retention) | Ref. |
|---|---|---|---|
| **$Fe_xO$@NFLG-240** | **423 mAh $g^{-1}$ at 50 mA $g^{-1}$, 226 mAh $g^{-1}$ at 2 A $g^{-1}$, 141 mAh $g^{-1}$ at 5 A $g^{-1}$** | **206 mAh $g^{-1}$ after 1000 cycles at 2 A $g^{-1}$, 140 mAh $g^{-1}$ after 5000 cycles at 5 A $g^{-1}$** | **This work** |
| Hybrid $Co_3O_4$-$Fe_2O_3$/C | - | 220 mAh $g^{-1}$ after 50 cycles at 50 mA $g^{-1}$ | Ref. [1] |
| $MoS_2$@rGO | 679 mAh $g^{-1}$ at 20 mA $g^{-1}$, 178 mAh $g^{-1}$ at 500 mA $g^{-1}$ | 381 mAh $g^{-1}$ after 100 cycles at 100 mA $g^{-1}$ | Ref. [2] |
| Bulk Bi | 406.6 mAh $g^{-1}$ at 40 mA $g^{-1}$, 321.6 mAh $g^{-1}$ at 1.2 A $g^{-1}$ | 321.6 mAh $g^{-1}$ after 300 cycles at 900 mA $g^{-1}$ | Ref. [3] |
| $Sn_4P_3$/C | 399.4 mAh $g^{-1}$ at 50 mA $g^{-1}$ 221.9 mAh $g^{-1}$ at 1 A $g^{-1}$, | 307.2 mAh $g^{-1}$ after 50 cycles at 50 mA $g^{-1}$ | Ref. [4] |
| Pistachio-Shuck-Like $MoSe_2$/C | 382 mAh $g^{-1}$ at 200 mA $g^{-1}$, 224 mAh $g^{-1}$ at 2 A $g^{-1}$ | 226 mAh $g^{-1}$ after 1000 cycles at 1 A $g^{-1}$ | Ref. [5] |
| NCNT | 254.7 mAh $g^{-1}$ at 50 mA $g^{-1}$ | 102 mAh $g^{-1}$ after 500 cycles at 2 A $g^{-1}$ | Ref. [6] |

| | | | |
|---|---|---|---|
| $VSe_2$ Nanosheet | 366 mAh $g^{-1}$ at 100 mA $g^{-1}$, 172 mAh $g^{-1}$ at 2 A $g^{-1}$ | 169 mAh $g^{-1}$ after 500 cycles at 2 A $g^{-1}$ | Ref. [7] |
| Hard Carbon derived from $NH_2$-MIL-101(Al) | 365 mAh $g^{-1}$ at 25 mA $g^{-1}$, 118 mAh $g^{-1}$ at 3 A $g^{-1}$ | 130 mAh $g^{-1}$ after 1100 cycles at 1.05 A $g^{-1}$ | Ref. [8] |
| Ultra-High Pyridinic N-Doped Porous Carbon Monolith | 225 mAh $g^{-1}$ at 1 A $g^{-1}$ | 150 mAh $g^{-1}$ after 3000 cycles at 1 A $g^{-1}$ | Ref. [9] |
| Nitrogen-rich hard carbon | 180 mAh $g^{-1}$ at 500 mA $g^{-1}$ | 170 mAh $g^{-1}$ after 4000 cycles at 500 mA $g^{-1}$ | Ref. [10] |

# Reference


1. I. Sultana, M. M. Rahman, S. Mateti, V. G. Ahmadabadi, A. M. Glushenkov and Y. Chen, *Nanoscale*, 2017, **9**, 3646-3654.
2. K. Xie, K. Yuan, X. Li, W. Lu, C. Shen, C. Liang, R. Vajtai, P. Ajayan and B. Wei, *Small*, 2017, **13**, 1701471.
3. K. Lei, C. Wang, L. Liu, Y. Luo, C. Mu, F. Li and J. Chen, *Angew. Chem., Int. Ed.*, 2018, **57**, 4687-4691..
4. W. Zhang, J. Mao, S. Li, Z. Chen and Z. Guo, *J. Am. Chem. Soc.*, 2017, **139**, 3316-3319.
5. W. Wang, B. Jiang, C. Qian, F. Lv, J. Feng, J. Zhou, K. Wang, C. Yang, Y. Yang and S. Guo, *Adv. Mater.*, 2018, **30**, 1801812.
6. P. Xiong, X. Zhao and Y. Xu, *ChemSusChem*, 2018, **11**, 202-208.
7. C. Yang, J. Feng, F. Lv, J. Zhou, C. Lin, K. Wang, Y. Zhang, Y. Yang, W. Wang, J. Li and S. Guo, *Adv. Mater.*, 2018, **30**, 1800036.
8. J. Yang, Z. Ju, Y. Jiang, Z. Xing, B. Xi, J. Feng and S. Xiong, *Adv. Mater.*, 2018, **30**, 1700104.
9. Y. Xie, Y. Chen, L. Liu, P. Tao, M. Fan, N. Xu, X. Shen and C. Yan, *Adv. Mater.*, 2017, **29**, 1702268.
10. C. Chen, Z. Wang, B. Zhang, L. Miao, J. Cai, L. Peng, Y. Huang, J. Jiang, Y. Huang, L. Zhang and J. Xie, *Energy Storage Mater.*, 2017, **8**, 161-168.